Proc. Natl. Acad. Sci. USA
Vol. 96, pp. 465–470, January 1999
Biophysics

Observation of transient disorder during myosin subfragment-1 binding to actin by stopped-flow fluorescence and millisecond time resolution electron cryomicroscopy: Evidence that the start of the crossbridge power stroke in muscle has variable geometry

MATTHEW WALKER*, XUE-ZHONG ZHANG†, WEI JIANG‡, JOHN TRINICK*, AND HOWARD D. WHITE‡§

*School of Biomedical Sciences, Leeds University, Leeds LS2 9JT, United Kingdom; †Enzyme Engineering Laboratory, Jilin University, Changchun, China; and ‡Department of Biochemistry, Eastern Virginia Medical School, Norfolk, VA 23507

Communicated by William P. Jencks, Brandeis University, Waltham, MA, November 19, 1998 (received for review June 23, 1998)

ABSTRACT **The mechanism of binding of myosin subfragment-1 (S1) to actin in the absence of nucleotides was studied by a combination of stopped-flow fluorescence and ms time resolution electron microscopy. The fluorescence data were obtained by using pyrene-labeled actin and exhibit a lag phase. This demonstrates the presence of a transient intermediate after the collision complex and before the formation of the stable "rigor" complex. The transient intermediate predominates 2–15 ms after mixing, whereas the rigor complex predominates at time >50 ms. Electron microscopy of acto-S1 frozen 10 ms after mixing revealed disordered binding. Acto-S1 frozen at 50 ms or longer showed the "arrowhead" appearance characteristic of rigor. The most likely explanation of the disorder of the transient intermediate is that the binding is through one or more flexible loops on the surfaces of the proteins. The transition from disordered to ordered binding is likely to be part of the force-generating step in muscle.**

The primary force-producing event of muscle contraction is thought to be a gross conformational change in the heads of the myosin (M) molecule whilst attached to actin (A) (1, 2); however, the structural and biochemical steps in this mechanism are not well understood. The tightly bound actomyosin (AM) complex that forms in the absence of nucleotides and probably corresponds to the end of the power-stroke has been described to ≈3-nm resolution (3). In smooth muscle, another tightly bound AM complex in ADP has been shown to have a substantially different conformation (4). However, the conformation(s) of the earlier stages in the power-stroke are not known. For instance, it is not known whether the start of the power-stroke has only one conformation, nor is it known whether the various transient intermediates that can be identified by solution kinetics are associated with particular conformations.

The biochemistry of the interaction between actin and myosin subfragments has been studied *in vitro* by a variety of methods, including binding, stopped-flow, and pressure relaxation (5–7). Intermediates of the ATP hydrolysis mechanism have been classified into two broad categories according to actin affinity, weak and strong (8, 9), and the force-producing step is thought to involve conversion from weak to strong binding. Thus myosin subfragment-1 (S1) binds strongly to actin in the absence of nucleotide or with ADP in the active site, but the binding is approximately 10^4 weaker with either ATP or ADP and P_i present. Geeves and coworkers have shown that S1 and S1-ADP bind to actin by a two-step mechanism and proposed that the initial transient state is similar to the weak state formed when either ATP or ADP and P_i are in the active site. The weak and rigor states have often been referred to as the A and R states, respectively (10).

The conformations of the weakly bound complexes have been little studied, in large part because they tend to dissociate at the low protein concentration feasible for electron microscopy of solutions. We have used low ionic strength to stabilize these complexes and previously observed that binding during steady-state ATP hydrolysis has a wide distribution of angles (11). This disorder might be explained by a mixture of the biochemical states AM-ATP and AM-ADP-P_i during steady-state hydrolysis. However, disorder was also observed 5 ms after mixing AM with ATP (12). In these experiments, there was no time for significant hydrolysis to occur and thus AM-ATP was the predominant intermediate. The rates of S1-ADP-P_i binding to actin and of steady-state ATP hydrolysis both have the same dependence on ionic strength, which provides evidence that intermediates at low ionic strength are on the kinetic pathway of the hydrolysis mechanism (6, 12). However, it has also been suggested that the effect of lowering the ionic strength is to populate collision complexes (13), in which case the structures seen under these conditions would be formed before the power-stroke.

Here we report parallel stopped-flow fluorescence and electron microscopy studies of the kinetic mechanism of S1 binding to actin in the absence of nucleotide. The stopped-flow studies were done by using actin, to which a pyrene group was covalently attached to CYS-374. The pyrene fluorescence provides a sensitive indicator of the isomerization step of the two-step binding reaction (14). The data show that a transient intermediate, which is clearly differentiated from the collision complex, forms within a few ms and is then converted at a slower rate to the rigor complex. Electron micrographs of the complex at early times after mixing were obtained by spraying S1 onto grids layered with actin immediately before freezing. Disordered binding was observed 5 ms after mixing and was followed by conversion to ordered binding after 50 ms. The appearance of the disordered intermediate is similar to that observed when S1 binds to actin in the presence of nucleotides (M-ATP and M-ADP-P_i) (11, 12). These results suggest that the transient intermediate that most nearly corresponds to the start of the power stroke does not have a single conformation.

MATERIALS AND METHODS

Protein Preparation. Rabbit skeletal muscle actin, myosin, and myosin-S1 were prepared as previously described (6). Crude S1 was purified on a DEAE-52 cellulose column and

The publication costs of this article were defrayed in part by page charge payment. This article must therefore be hereby marked "*advertisement*" in accordance with 18 U.S.C. §1734 solely to indicate this fact.

PNAS is available online at www.pnas.org.

Abbreviations: S1, myosin subfragment-1; M, myosin; A, actin; AM, actomyosin; HMM, heavy meromyosin.

§To whom reprint requests should be addressed. e-mail: white@borg.evms.edu.

fractions were pooled to obtain only the A1 light chain isomer (15). Actin was labeled with pyrene–iodoacetamide (Molecular Probes) by the procedure of Criddle *et al.* (10). The labeling ratio determined spectroscopically was 0.8 to 0.9 pyrene per actin. The maximum steady-state rates of actin-activated ATP hydrolysis of the S1 were the same within experimental error for control and pyrene-actin, but K_{app} was two to three times larger with pyrene-actin. This suggests a slightly reduced affinity of pyrene-actin to S1 during steady-state hydrolysis. G-actin and pyrene-G-actin were stored at −80°C by drip-freezing into liquid nitrogen. Before use, the G-actin solutions at 4–8 mg/ml were thawed and polymerized by dialysis overnight against 100 volumes of 5 mM Mops/2 mM $MgCl_2$/0.5 mM DTT, pH 7.0, 4°C. F-actin was diluted to 2 μM in the same buffer and residual ATP and ADP were removed by treatment with 0.01 units per ml of apyrase (Sigma A6535) for 15 minutes.

Kinetic Methods. Presteady-state measurements of changes in fluorescence were made with a stopped-flow fluorimeter (Applied Photophysics, Surrey, U.K.). The flow cell was illuminated on the 1 × 2-mm port by a 100-watt mercury arc lamp. The excitation wavelength, 365 nm for pyrene-actin, was selected with a 12.4-cm monochrometer (Farrand) and emission by a 418-nm cutoff filter. The voltage output of the photomultiplier was smoothed with a one-stage active filter with a time constant of 100 μsec. The data from four 1,024-point traces measured at equal time increments were recorded with a Nicolet Explorer III digital oscilloscope, transferred to a personal computer, averaged, and stored. These data were then further averaged to approximate a logarithmic timebase to provide equal weighting of slow and fast components when fitting data to more than one exponential (16). The first 16 points after 1 ms were not averaged, the next 32 points were averaged to 16 points, the next 64 points averaged to 16 points, etc., to obtain a total of 96 points from the original 1,024 data points.

Before some stopped-flow experiments, equimolar concentrations of phalloidin and pyrene-actin were incubated for 1 hr because of concern that depolymerization of the actin (and/or repolymerization by S1) might produce kinetic artifacts. Although the total signal amplitudes were larger in the presence of phalloidin, the observed rate and fractional amplitudes were the same within experimental error, and thus phalloidin was not used routinely.

At concentrations of <10 μM S1, the data were not fit well by a single exponential equation, but were by an irreversible two-step kinetic mechanism (A → B → C) in which the fluorescence change occurred only with formation of the final product (C). The initial fitting was used to determine the concentration dependence of the observed rate constants for conventional data analyses and to scale the data for global fitting. A stiff episode integrator and a nonlinear least squares fitting routine in the software package SCIENTIST (Micromath, Salt Lake City, UT) were used to determine kinetic constants by global fitting of the stopped-flow data. The initial binding step K_0 was assumed to be in rapid equilibrium ($k_{-0} \gg k_1$). K_0 and values for the rate constants k_1, k_{-1}, and k_2 were determined by global fitting data from the entire range of S1 concentrations at the same time to differential equations describing the mechanism in Eq. **1**.

$$A + M \overset{K_0}{\rightleftharpoons} AM_0 \underset{k_{-1}}{\overset{k_1}{\longrightarrow}} AM_1 \underset{k_{-2}}{\overset{k_2}{\longrightarrow}} AM_2 \qquad [1]$$

Global fitting to determine the rate constants of a kinetic mechanism provides more discriminating evidence for the mechanism than fitting apparent rate constants separately to each concentration, because the correct dependence of both the relaxation times and amplitudes is required.

Time-Resolved Electron Cryomicroscopy. The method for preparing specimens for time-resolved electron cryomicroscopy is similar to that described by Berriman and Unwin (17) and involves layering one reactant onto a microscope grid and then spraying on a second reactant immediately before freezing. The apparatus that we have built consists of a holey carbon grid held by forceps mounted on a pneumatic piston (12, 18). The grid is layered with actin and then blotted by gentle squeezing from both sides by filter papers, which are mounted on soft pads that are also driven by pneumatic pistons. At 50 ms after withdrawal of the filter papers, the grid is propelled at ≈2 m/s into liquid ethane maintained near its melting point (−172°C). Just before entering the ethane, the grid passes through a spray containing the S1. Small droplets of myosin-S1 averaging 0.5 μm diameter are produced by an atomizer (model 3076, TSI, St. Paul) supplied with humidified nitrogen at 2.5 bar, which produces a jet through a small aperture (enlarged to 0.7 mm from the 0.35 mm supplied). The flow of myosin-S1 into the atomizer is accurately controlled by a microstepper motor-driven syringe pump. The number of spray droplets that arrive on the grid is increased ≈5× by biasing the spray output nozzle +7 kV with respect to the grid, which is grounded. Although melting ethane has a very low vapor pressure, extreme care was taken when using it with high voltages. Timing signals for the solenoids controlling the spray, pistons, and the high voltage were generated with millisecond precision by a custom Windows program written in Visual Basic (Dover Software, Hampstead, U.K.). Signals from the data lines of the printer port of a personal computer were used to control an optical interface that electrically isolates the computer. The rate of movement of a series of 1-mm black bars at intervals of 1 mm on a thin piece of clear plastic (attached to the forceps supporting the electron microscopy grid) through a photodiode/phototransistor combination was used to time the descent of the grid. The micrographs presented here were all obtained from grids sprayed at 4°C in the cold room. A more complete description of the apparatus is published elsewhere (18).

Grids were examined by using a Gatan model 626 (Gatan, Pleasanton, CA) cold-specimen holder in a Jeol 1200ex microscope operating at 80 kV with a modified anticontaminator. Areas over holes were photographed at ×46,000 by using low-dose (≈10 e/Å^2) and a defocus of 3 μm. Colloidal gold particles (5 or 10 nm) coupled to BSA (Biocell Laboratories) were included in the spray at final concentrations of 2×10^{14} and 2.3×10^{13} particles per ml respectively to aid searching at ×8,000 for areas that had received a spray droplet.

RESULTS

Kinetics of S1 Binding to Pyrene-Actin. Fig. 1 shows the decrease in fluorescence observed when pyrene-labeled actin was mixed with a series of concentrations of S1 in a stopped-flow fluorimeter. The data points (black squares) are plotted against the logarithm of time to make it easier to determine the quality of curve fitting over the entire time course. The data are fit poorly by a mechanism in which the conversion of AM_0 to AM_1 is in rapid equilibrium: k_{-1} was held $\gg k_2$ and the fit was obtained to K_0, k_1, and k_2 (dashed lines). In contrast, the data are fit very well by a mechanism in which the collision complex is followed by two essentially irreversible steps ($k_{-1} < k_2$). The solid lines are theoretical curves obtained from the values in Eq. **2** obtained by globally fitting K_0, k_1, k_{-1}, and k_2 to the entire data set in Fig. 1.

$$\underset{<4 \times 10^4\ M^{-1}}{K_0} \quad \underset{>1{,}000\ s^{-1}}{k_1} \quad \underset{60\ s^{-1}}{k_{-1}}$$

$$A + M \rightleftharpoons AM_0 \longrightarrow AM_1 \longrightarrow AM_2 \qquad [2]$$

$$\underset{<20\ s^{-1}}{k_{-1}} \quad \underset{0.1-2\ s^{-1}}{k_2}$$

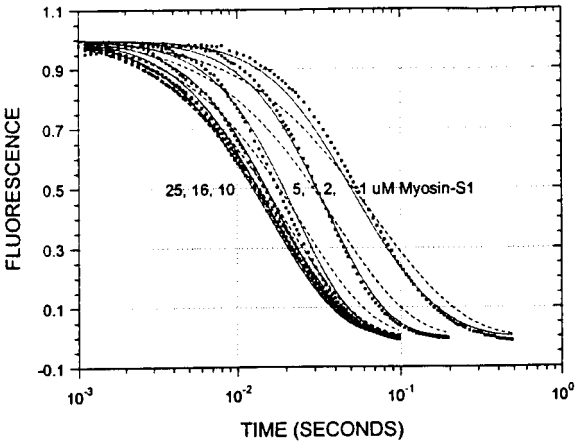

FIG. 1. Stopped-flow kinetic measurements of myosin-S1 binding to pyrene-actin. The decrease in pyrene fluorescence was observed on mixing myosin-S1 with pyrene-actin. The samples were excited at 365 nm and fluorescence emission was measured at >420 nm. The dashed lines drawn through the data are computer fits to a rapid equilibrium mechanism. The solid lines are fits to an irreversible binding mechanism that were calculated from the rate constants in Eq. **2**. Conditions: 0.5 μM pyrene-actin, the indicated concentration of myosin-S1 in 5 mM Mops/2.0 mM $MgCl_2$/0.5 mM DTT, pH 7.0 at 4°C.

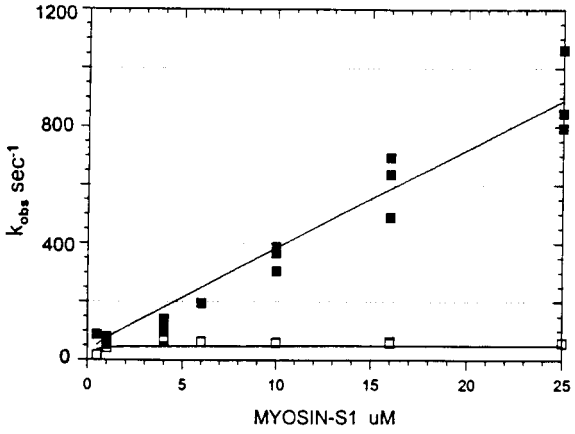

FIG. 2. Dependence of the observed rate constants on S1 concentration. The solid squares are for the step associated with the lag and the open squares for the fluorescence change step. Observed rate constants were obtained from three data sets similar to those described in Fig. 1. The theoretical lines through the data are from the mechanism shown in Eq. **2**.

The best fit of the lag in the fluorescence data gave a value of $\approx 1\ s^{-1}$ for k_{-1}. However, values of k_{-1} of up to $20\ s^{-1}$ produce only a small increase in the rms error of the fits and $20\ s^{-1}$ is an upper limit for k_{-1}. The second-order rate constant for S1 binding to actin, K_0k_1, is $4 \times 10^7\ M^{-1}\ s^{-1}$. Only limits can be obtained for the individual values of K_0 and k_1 (Eq. **2**). The overall association constant of S1 to actin ($K_a = K_0k_1/k_{dissoc} = 2 \times 10^9\ M^{-1}$) can be determined from the observed rate constant of dissociation of pyrene-acto-S1 in excess unlabeled actin (data not shown), which was $\approx 0.02\ s^{-1}$. Although a value for k_{-2} cannot be measured directly, $k_{-1} \cdot k_{-2} \approx 2$, is calculated from K_a and the other rate and equilibrium constants in Eq. **2**. Values for k_{-2} from 0.1 to 2 are estimated from the best fit and limiting values for k_{-1}.

Conventional analyses of the data were also done in which single and double exponential fits were made to the data separately at each concentration. The data were poorly fit by attempts at single exponential fitting, especially at concentrations <10 μM, which are similar to the dashed lines in Fig. 1. Double exponential fits in which the amplitudes for the two terms are of opposite sign (the arithmetic expression for a lag) were similar to the solid lines in Fig. 1. A similar lag in the fluorescence was previously observed by Taylor (7). Fig. 2 shows the concentration dependence of the fast and slow rate constants obtained from the two exponential fits. The observed rate of the lag has a linear dependence on S1 concentration up to $1{,}000\ s^{-1}$. The second slower step reaches a maximum of $60\ s^{-1}$ and is essentially independent of S1 concentration under these experimental conditions.

In summary, both global fitting and conventional kinetic analysis of the stopped-flow data indicate a multistep binding mechanism of S1 to actin. A collision complex is followed by rapid and essentially irreversible conversion to a short-lived intermediate, AM_1, which undergoes a slower isomerization to the equilibrium complex, AM_2. These results are in general agreement with those previously obtained for two-step binding of myosin-S1 to actin under somewhat different conditions (7, 14). An important additional feature is that the rate of reversal of AM_1 to A and M ($k_{-1} < 20\ s^{-1}$) is slow; thus AM_1 cannot be a collision complex, which would have a much more rapid rate of dissociation. Additional evidence for AM_1 not being a collision complex could be obtained if the maximum rate of its formation could be measured, but the maximum observed rate constant >$1{,}000\ s^{-1}$ is at the limit of stopped-flow measurements. However, in similar experiments measuring S1-ADP binding to pyrene-actin, K_0k_1 is $\approx 10^6\ M^{-1}\ s^{-1}$, k_1 is $\approx 100\ s^{-1}$, and k_2 is $\approx 60\ s^{-1}$ (data not shown). The simplest explanation for the effect of ADP on the binding mechanism is that k_1 is reduced by 40-fold without significantly changing K_0 or k_2. K_0, the equilibrium constant for the formation of the collision complex, AM_0, is approximately $10^4\ M^{-1}$ in the presence of ADP and if K_0 is similar in the absence of ADP, k_1 is $\approx$4000 s^{-1} in the absence of ADP. The rate of S1-ADP binding to actin is not diffusion limited nor is it likely to be in the absence of ADP.

The rate and equilibrium constants in Eq. **2** can be used to estimate the time course of formation and breakdown of AM_0, AM_1, and AM_2 for concentrations of actin and S1 approximating those during preparation of samples for microscopy. The concentration of S1 in the center of the region where a droplet collides with the grid was estimated to be $\approx$25 μM based on the number of gold particles visible. The inserts in Figs. 3 and 5 show the time dependence of the reaction species for 25 μM S1 binding to 2 μM actin. From 2 to 15 ms the predominant species is AM_1, whereas at >50 ms it is AM_2. The kinetics of formation and decay of AM_1 and AM_2 are not very sensitive to concentrations of [S1] >10 μM; [S1] <10 μM reduces the temporal resolution between the two intermediates. However, it should be noted that the binding kinetics after the collision of a droplet of S1 on a grid containing a film of actin will not be as simple or uniform as the kinetics observed in a stopped-flow cell, because the mixing is not homogeneous and the concentrations of S1 and actin will change with distance and time as the droplet diffuses. This may cause small deviations in the time course of the reaction on the electron microscope grid from that observed in bulk solution.

Time-Resolved Electron Cryomicroscopy. Fig. 3 shows a micrograph obtained by spraying actin (4 μM) with S1 (120 μM) $\approx$5 ms before being frozen. About 40% of the available actin filament length is unlabeled and in these regions the 5.5-nm subunit spacing and $\approx$35-nm long-pitch helical crossovers are clearly visible. Most of the length of the filaments is, however, decorated with particles having a size consistent with molecules of S1. These particles can also be seen in the background, and since they are not present in grids containing actin alone (not shown), we conclude that they are indeed S1 molecules. The attachment of the S1 on the actin is disordered and very different from the ordered "arrowhead" appearance that characterizes steady-state binding seen in ADP or in the

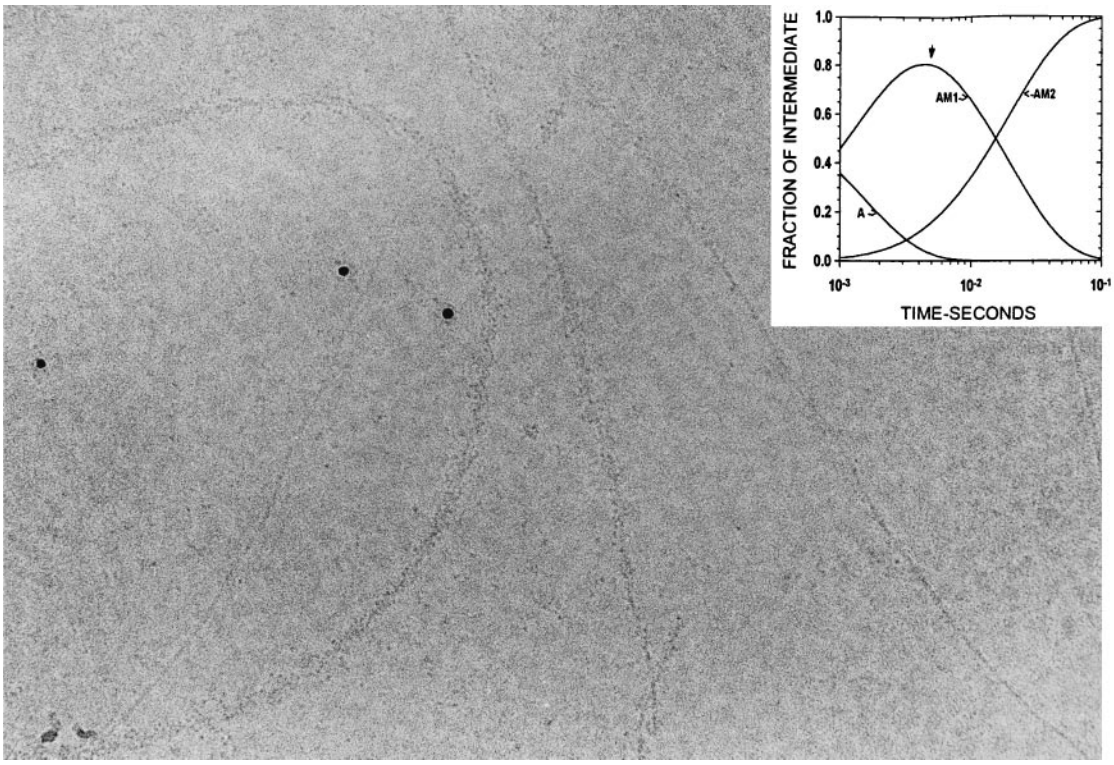

FIG. 3. Electron micrograph of actin sprayed with S1 5 ms before freezing. The S1 bound to the actin is disordered. There is also some S1 visible in the background that has not bound to actin filaments, as well as bare actin filaments. The characteristic subunit and helical substructure is clearly visible in the bare actin filaments. The six intensely black round particles are 5-nm colloidal gold that was included in the spray to aid in searching for areas of the grid that had received spray droplets. Some clustering of the S1 around the gold particles was seen; this depended on the particular batch of gold used and probably resulted from incomplete coverage of the BSA coupled to the gold. The insert shows the time course of the reaction intermediates calculated from the mechanism in Eq. **2** with an arrow indicating the time of freezing. Experimental conditions: 5 mM Mops/2.0 mM $MgCl_2$/0.5 mM DTT, pH 7.0, 4°C. (×388,000.)

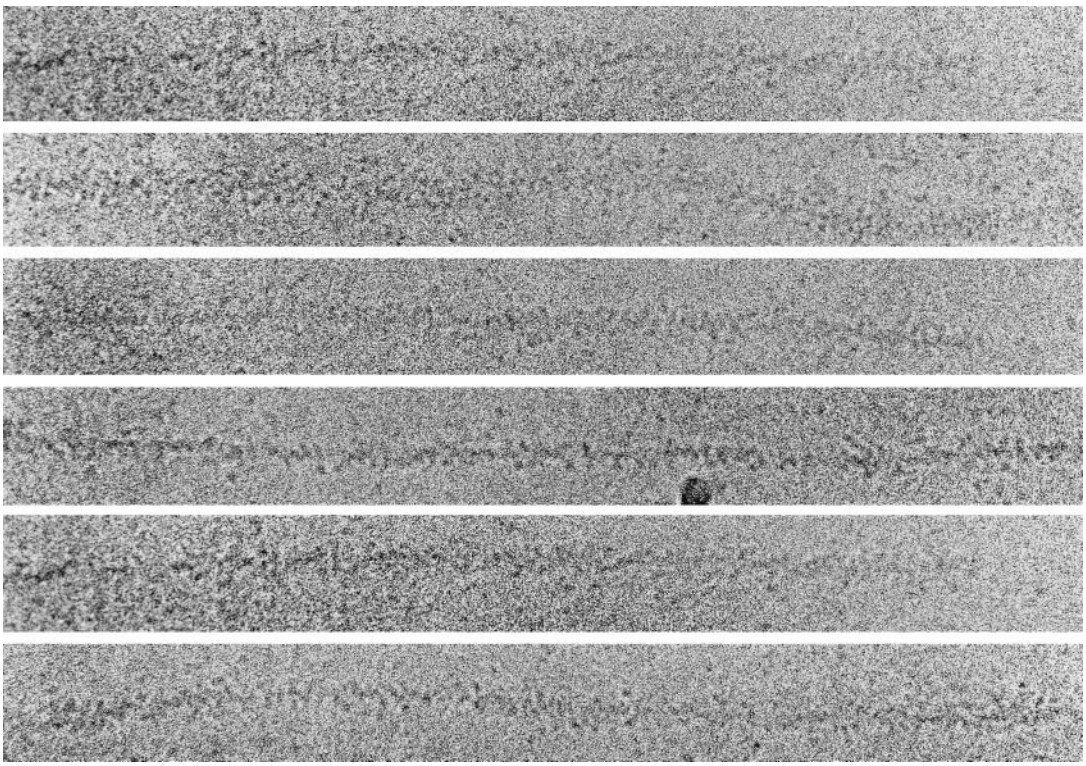

FIG. 4. Montage of actin with bound S1 frozen 5 ms after mixing as in Fig. 3. (×388,000.)

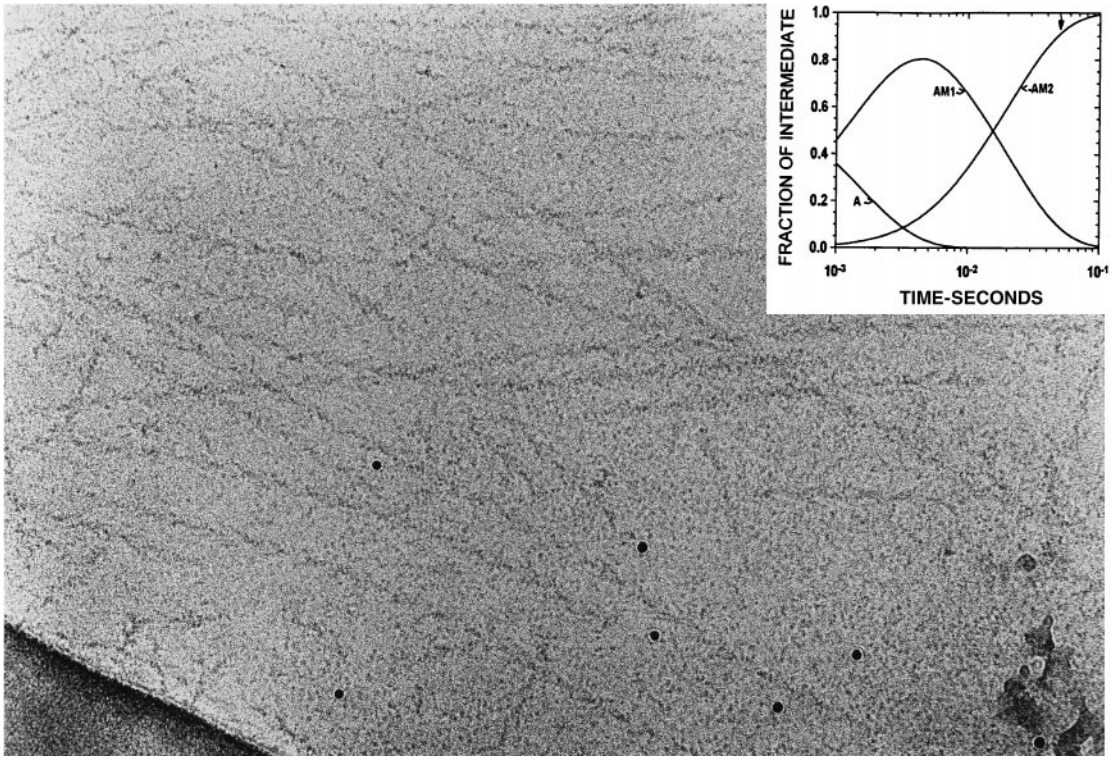

FIG. 5. Actin sprayed with S1 with a delay of 50 ms between spraying and freezing. The bound S1 now has the characteristic arrowhead appearance seen in the steady-state binding of S1 to actin in the absence of nucleotide. The arrow in the insert at 50 ms is at the time the sample in this micrograph was frozen. (×388,000.)

absence of nucleotide. Also visible in the micrograph are 5-nm colloidal gold particles; these are included in the spray and are used during low magnification (×8,000) searching to locate areas of the grid that have received a spray droplet. Fig. 4 shows a montage of similar actin filaments labeled by S1 sprayed 5 ms before freezing. In all cases the binding was disordered.

Fig. 5 shows a micrograph from a grid sprayed with S1, in which the delay between spraying and freezing was 50 ms and in which the main intermediate (>90% as shown by the arrow in the insert) is expected to be AM_2. Although there are still some S1 molecules in the background, most of the actin now has S1 bound and clearly shows evidence of the ordered arrowhead appearance seen in rigor binding. The difference between the disordered and ordered binding is most easily viewed by looking down the filament axis at an oblique angle.

DISCUSSION

A large conformational change in the attached myosin head remains the most likely origin of muscle force. To understand this mechanism, it is therefore essential to determine the conformation of the crossbridge at different stages of its power stroke, and it is particularly important to define the beginning and end of the stroke. The tightly bound states of the acto-S1 complex, with ADP or no nucleotide present, are the only attached states with conformations that have been described in detail and are thought to be formed near the end of the power stroke (3, 4). Earlier stages in the stroke occurring with ATP or ADP·P_i bound to myosin are more difficult to study, mainly because of their low affinity, and work done to examine these complexes directly by electron microscopy has given conflicting results. Most studies have used specimens that were frozen, cleaved, etched, and then rotary shadowed. Using this approach, Pollard *et al.* found no change in the conformation of S1 on actin in the presence or absence of ATP, which led them to reinforce earlier suggestions that nontilting crossbridge models of force production should be explored further (19). In a similar experiment, Funatsu *et al.* also found no major changes, but reported a broader distribution of attachment angles in ATP (20). However, also using freeze-etching and shadowing, Katayama (21) reported a large change in the shapes of both attached and detached heads of both S1 and heavy meromyosin (HMM) in ATP; these differences from the other studies were attributed to preabsorption of the proteins onto mica flakes resulting in better resolution, both by supporting the molecules and by avoiding shadowing from both sides. Frado and Craig observed disordered binding of HMM to F-actin by negative staining in the presence of ATP (22) and Flicker and Applegate observed disordered binding of S1 to actin by negative staining and electron-microscopy (23). It can be questioned, however, whether S1 retains enzyme activity and native structure in negative stain and whether the covalent crosslinks merely provide a flexible tether for dissociated crossbridges.

The advantage of the vitrified specimens used here is that they remain hydrated throughout at < -165°C, where there is no opportunity for the conformation of the proteins to be modified. This could conceivably happen in preparation of shadowed specimens, for instance when the water crystallizes (at ≈ -150°C) or is sublimed (at ≈ -100°C), or when the metal coat is applied. The introduction of the spray method for preparing hydrated specimens further extends this approach to allow the exploitation of fast freezing for time-resolved studies. Because a wide variety of solutes can be delivered in sprays, from small molecules to proteins and even macromolecular assemblies, this approach provides a general method for studying the conformations of transient reaction intermediates of proteins. It is thus possible to correlate kinetic data obtained in bulk solution with ms time resolution microscopy. Until now, the spraying method has been used to study the effects of small molecules on proteins, (17, 11, 24), but it can also be used to study protein–protein interactions, as described here.

A few milliseconds after mixing, the arrangement of the S1 on actin is disordered; this is followed by a transition to the ordered tightly bound state within 50–100 ms. This time course is very similar to the time course of binding monitored by changes in pyrene fluorescence observed by stopped flow. The kinetic data show that an intermediate, AM_1, is formed rapidly and irreversibly from the collision complex; this is then less rapidly converted to AM_2. At times between 2 and 15 ms, AM_1 is the predominant kinetic intermediate and thus the electron microscopy shows that AM_1 is disordered.

Our experiments were carried out at very low ionic strength, which was used to maximize the rate of formation of AM_1, so that AM_1 and AM_2 can be kinetically resolved. Previously we have also observed similar disordered binding in low salt concentrations during steady-state hydrolysis and $\approx$5 ms after binding of mant-ATP to acto-S1. Whether the conformations observed in low salt are directly related to force production has been questioned previously (13). It was suggested that the apparent lack of stereospecific binding could be explained if the effect of lowering the ionic strength was to populate the collision state. We show here that AM_1 is a kinetically competent intermediate formed irreversibly after the collision state and before the final rigor complex. A possible mechanism for the disordered binding is a flexible attachment between negative charges on the C terminus of actin and positive charges in the loop 2 region of the myosin 50K/20K junction (25). There are experimental data obtained by several different methods indicating that a transition from disordered to ordered binding of the myosin head while attached to actin produces the power stroke. ESR studies of AM-S1 in solution, myofibrils, and fibers all indicate that a large fraction of myosin heads in contracting muscle fibers are weakly bound to actin and are disordered and highly mobile on the microsecond time scale (26–28). X-ray diffraction and mechanical studies support this view (29, 30).

Previous estimates of the equilibrium constant for the transition from AM_1 to AM_2 are approximately 200 (7, 14), which is similar to what we have found between the collision complex AM_0 and AM_1, which is $>$50. The free energy changes between the collision complex and the final rigor complex are therefore divided approximately equally between the two transitions AM_0 to AM_1 and AM_1 to AM_2. Thus, energetically, the AM_1 state is not at the start of the mechanism, which also argues against it being a collision state. The equilibrium constant for the formation of AM_1 measured here, $>10^6$ M^{-1}, is similar to that measured for M-ATP binding to actin (10^6 M^{-1}) but stronger than that of M-ADP-P_i ($5{\cdot}10^4$ M^{-1}) (31).

Our data are consistent with the model in which binding of S1 to actin is always a multistep process, whatever nucleotide is bound, and with the transition from weak to strong binding being the force-generating event (32). The complexities of the product- dissociation kinetics that follow binding of M-ADP-P_i to actin, as occurs in muscle, make detailed kinetic analysis similar to that which we have done here in the absence of nucleotide extremely difficult. But it is likely that the effect of the bound products on myosin is to modify the kinetics of the reaction rather than the reaction pathway. Ishigima *et al.* have recently shown by a combination of single-molecule fluorescence and force measurements that myosin heads are able to bind actin and produce the same amount of force after the products ADP and phosphate have dissociated as when products are bound to the myosin (33). Thus, it is likely that the AM_1 state is similar to the weak binding state postulated as the start of the power-stroke. Although it is natural to assume that the start of the power stroke has only one conformation, there is no *a priori* reason why this should be the case. Here we provide direct evidence that the start of the power-stroke has more than one conformation.

We thank Betty Belknap for preparing S1 and actin, Debbie Kelly for help in developing procedures using SCIENTIST to analyze the kinetic data, and Peter Knight for critically reading the manuscript. This work has been supported by research grants from the U.K. Medical Research Council and the National Institutes of Health (AR40964).

1. Huxley, H. E. (1969) *Science* **164,** 1356–1366.
2. Huxley, A. F. & Simmons, R. M. (1971) *Nature (London)* **223,** 533–538.
3. Milligan, R. A. & Flicka, P. F (1987) *J. Cell. Biol.* **105,** 29–39.
4. Whittaker, M., Wilson-Kubalek, E. M., Smith, J. E., Faust, L., Milligan, R. A. & Sweeney, H. L. (1995) *Nature (London)* **378,** 748–751.
5. Highsmith, S. (1976) *J. Biol. Chem.* **251,** 6170–6172.
6. White, H. D. & Taylor, E. W. (1976) *Biochemistry* **15,** 5818–5825.
7. Taylor, E. W. (1991) *J. Biol. Chem.* **266,** 294–302.
8. Eisenberg, E. & Greene, L. E. (1980) *Annu. Rev. Physiol* **42,** 293–309.
9. Geeves, M. A. (1992) *Philos. Trans. R. Soc. London B* **336,** 63–71.
10. Criddle, A. H., Geeves, M. A. & Jeffries, T. (1985) *Biochem. J.* **232,** 343–349.
11. Walker, M., White, H., Belknap, B. & Trinick, J. (1994) *Biophys. J.* **66,** 1563–1572.
12. Walker, M., Trinick, J. & White, H. (1995) *Biophys. J.* **68,** 87s–91s.
13. Holmes, K. C. (1996) *Curr. Opin. Struct. Biol.* **6,** 781–789.
14. Coates, J. H., Criddle, A. H. & Geeves, M. A. (1985) *Biochem. J.* **232,** 351–356.
15. Weeds, A. G. & Taylor, R. S. (1975) *Nature (London)* **257,** 54–56.
16. Walmesley, A. R. & Bagshaw, C. R. (1989) *Anal. Biochem.* **176,** 313–318.
17. Berriman, J. & Unwin, N. (1994) *Ultramicroscopy* **56,** 241–252.
18. White, H. D., Walker, M. L. & Trinick, J. (1998) *J. Struct. Biol.* **121,** 306–313.
19. Pollard, T. D., Bhandari, D., Maupin, P., Wachsstock, D., Weeds, A. G. & Zot, H. G. (1993) *Biophys. J.* **64,** 454–471.
20. Funatsu, T., Kono, E. & Tsukita, S. (1993) *J. Cell Biol.* **121,** 1053–1064.
21. Katayama, E. (1998) *J. Mol. Biol.* **278,** 349–367.
22. Frado, L. L. & Craig, R. (1992) *J. Mol. Biol.* **223,** 391–397.
23. Flicker, P. & Applegate, D. (1987) *J. Biol. Chem.* **262,** 6856–6863.
24. Fuller, S. D., Berriman, J. A., Butcher, S. J. & Gowar, B. E. (1995) *Cell* **81,** 715–725.
25. Rayment, I., Holden, H. M., Whittaker, M., Yohn, C. B., Lorenz, K. C., Holmes, K. C. & Milligan, R. A. (1993) *Science* **261,** 58–65.
26. Berger, C. L. & Thomas, D. D. (1994) *Biophys. J.* **67,** 250–261.
27. Fajer, P. G., Fajer, E. A., Schoenberg, M. & Thomas, D. D (1991) *Biophys. J.* **60,** 642–649.
28. Zhao, L., Naber, N. & Cooke, R. (1995) *Biophys. J.* **68,** 1980–1990.
29. Yu, L. C. & Brenner, B. (1989) *Biophys. J.* **55,** 441–453.
30. Lowy, J. & Poulsen, F. R. (1987) *J. Mol. Biol.* **194,** 595–600.
31. White, H. D., Belknap, B. & Webb, M. R. (1997) *Biochemistry* **36,** 11828–11836.
32. Geeves, M. A., Goody, R. S. & Gutfreund, H. (1984) *J. Muscle Res. Cell Motil.* **5,** 351–361.
33. Ishijima, A., Kojima, H., Funatsu, T., Tokunaga, M., Higuchi, H., Tanaka, H. & Yanagida, T. (1998) *Cell* **92,** 161–171.